Peregrine solitons and resonant radiation in cubic and quadratic media

Marcos Caso-Huerta
Department of Information Engineering
University of Brescia, Italia
Email: marcos.casohuerta@unibs.it

Lili Bu
School of Physics & Frontiers Science Center
for Mobile Information, Communication & Security
Southeast University, Nanjing, China
&
Department of Information Engineering
University of Brescia, Italy
Email: lili.bu@unibs.it

Shihua Chen
School of Physics & Frontiers Science Center
for Mobile Information, Communication & Security
Southeast University, Nanjing, China
&
Purple Mountain Laboratories, Nanjing, China
Email: cshua@seu.edu.cn

Stefano Trillo
Department of Engineering
University of Ferrara, Italy
Email: stefano.trillo@unife.it

Fabio Baronio
Department of Information Engineering
University of Brescia, Italy
Email: fabio.baronio@unibs.it

Abstract

We present the fascinating phenomena of resonant radiation emitted by transient rogue waves in cubic and quadratic nonlinear media, particularly those shed from Peregrine solitons, one of the main wavepackets used today to model real-world rogue waves. In cubic media, it turns out that the emission of radiation from a Peregrine soliton can be attributed to the presence of higher-order dispersion, but is affected by the intrinsic local longitudinal variation of the soliton wavenumber. In quadratic media, we reveal that a two-color Peregrine rogue wave can resonantly radiate dispersive waves even in the absence of higher-order dispersion, subjected to a phase-matching mechanism that involves the second harmonic wave, and to a concomitant difference-frequency generation process. In both cubic and quadratic media, we provide simple analytic criteria for calculating the radiated frequencies in terms of material parameters, showing excellent agreement with numerical simulations.

1 Introduction

The interest in the generation and manipulation of linear dispersive waves has spiked in recent years, with areas ranging from optical fibers [1, 2], photonic crystal fibers [3, 4], semiconductor waveguides [5, 6, 7] to microresonators [8, 9, 10, 11], because of their critical role in supercontinuum generation[12, 13] and frequency comb generation[14, 15, 16].

Starting from the most studied case of solitons arising from the balance of group velocity dispersion (GVD) and cubic (Kerr) nonlinearity, ruled by the nonlinear Schrödinger (NLS) equation, it is well known that solitons cannot be in resonance with linear waves since their wavenumbers are intrinsically different. Indeed solitons experience a nonlinear shift of their wavenumber which is of opposite sign compared to the GVD-induced shift of the wavenumber of linear waves. However, the situation changes when the contribution from higher-order dispersion becomes effective, which allows the soliton wavenumber to be equal to that of linear waves with suitable frequency detuning from the soliton central frequency. When such a resonant condition is fulfilled, linear dispersive waves at that frequency detuning can grow spontaneously, by taking energy at the expense of re-shaping of the propagating soliton. This phenomenon is usually termed resonant radiation (RR) [17, 18, 19, 20, 21, 22] or Cherenkov radiation [23], and its physical origin is essentially the same (apart from specific details) for solitons which are shape-invariant under unperturbed conditions, higher-order solitons (breathers with zero-background), breathers standing on non-zero background (such as the Peregrine solitons discussed in this paper), or cavity solitons. The net effect is that such wavepackets, which typically show great robustness, give rise to the spontaneous and persistent emission of linear radiation at certain characteristic frequencies detuned from the soliton spectral peak, typically ascribed to the presence of higher-order dispersive effects. RR has also been found to have played a relevant role in four-wave mixing phenomena [24, 25, 26] and in wave-breaking [27, 28, 29], among others. Furthermore, either built-in or intrinsic periodicity in the system can enhance the emission of RR featuring characteristic multiple spectral peaks under different pumping conditions [30, 31, 32].

We first treat the RR in cubic media [22], using the focusing NLS equation. We will focus on one of the most relevant rational solutions, the Peregrine soliton [33], which was first observed in nonlinear optics [34] but found to be ubiquitous in many branches of physics, including plasma physics[35] and hydrodynamics[36]. Peregrine solitons (oftentimes referred to as Peregrine breathers, as they appear as the infinite period limit for both Akhmediev and Kuznetsov-Ma breathers) are now thought of as the prototype of realistic rogue waves[37, 38, 39], as they are localized in both space and time and typically present an amplitude more than twice the significant wave height [34, 40, 41, 42]. Its universality relies also on the fact that Peregrine solitons appear as the local waveshape,

1

regardless of the original input shape, in the vicinity of the focusing catastrophe point occurring when nonlinearity dominates over GVD[43]. At variance with the radiation shed from classical shape-invariant bright or dark solitons, but similarly to that shed by higher-order solitons[44], for these exotic localized wavepackets the RR in cubic media is caused by the higher-order dispersions and affected by the intrinsic local longitudinal variation of the soliton wavenumber. The range of physical applications of the RR emitted by Peregrine solitons are very similar to those of classical solitons, but the different conditions for their generation and different regimes in which they operate may make the former RR more suitable for a given setting[45], thus considerably broadening the spectrum of applications.

We then consider the RR in quadratic media. In the past two decades, soliton-like pulses in quadratic media have been widely studied in the literature [46, 47, 48, 49, 50, 51, 52], and the RR from such solitons has been both theoretically predicted[53, 54, 55] and experimentally observed in bulk BBO crystals in the normal GVD regime and effectively defocusing nonlinearity [56, 57, 58, 59], as well as in periodically poled lithium niobate [60]. However, all these analytic predictions have been reliant on the existence of higher-order dispersion. Here we review our recent results on RR emitted by Peregrine solitons in quadratic media, both in the cascading and the phase-matching regimes. Contrary to the cubic case, where RR can only be driven by higher-order dispersion, in quadratic media there exists another potential mechanism responsible for the generation of linear dispersive waves. In latter situation, the RR occurs first at the second harmonic (SH) component, by phase-matching its linear frequency with the frequency of the Peregrine soliton, and in turn at the fundamental frequency (FF) component via a parametric down-conversion process [61, 62].

The subsequent sections are organized as follows. In Sec. 2, we present the Peregrine soliton solution of the cubic NLS equation containing third-order dispersion (TOD) and discuss the RR characteristics caused by TOD. In Sec. 3, we provide approximate Peregrine soliton solutions in quadratic media and demonstrate their RRs in both the cascading and non-cascading regimes. Finally, we conclude the review in Sec. 4.

2   Cubic media

We consider the following normalized form of the NLS equation, written in the usual notation for fiber optics:[22]

$$i\psi_\xi - \frac{\beta_1}{2}\psi_{\tau\tau} - i\frac{\sigma_1}{6}\psi_{\tau\tau\tau} + |\psi|^2\psi = 0, \tag{1}$$

where ψ represents the (complex) wave amplitude, $\tau = (t - z/v_g)/t_0$ and $\xi = z/z_{nl} = z\gamma P$ where t and z are the time and distance in the lab frame, and $t_0 = (|\beta''|z_{nl})^{1/2}$ and the nonlinear length $z_{nl} = (\gamma P)^{-1}$ are associated with the power P of the background and the Kerr effective coefficient γ; v_g is the group velocity for a carrier frequency ω_0 of the electric field $E(T, Z) = \sqrt{P}\psi(\xi, \tau)$, and $\beta_1 = \beta''/|\beta''|$ and $\sigma_1 = \beta'''/|\beta''|t_0$ are second and third-order dispersion coefficients, respectively.

In the integrable limit $\sigma_1 = 0$ under the anomalous regime $\beta_1 = -1$ (often referred to as focusing NLS), Eq. (1) admits the following rational Peregrine soliton over the unit background:[33]

$$\psi(\xi, \tau) = \left[1 - \frac{4(1 + 2i\xi)}{1 + 4\xi^2 + 4\tau^2}\right]\exp(i\kappa_b\xi), \tag{2}$$

where the exponential term comes from the nonlinear Kerr shift of the background. In our normalized setting, the background wavenumber is $\kappa_b = 1$ (which corresponds to $\kappa_b z_{nl}^{-1}$ prior to normalization), but henceforth we stick to generic κ_b to track its contribution.

This solution behaves as an initially weak pulse over the (unit) background that undergoes a single cycle of compression and growth to finally broaden and decay. This behavior in the time domain is sustained by a strong spectral broadening in the Fourier domain, which serves as a forcing mechanism to generate RR when its frequency is phase-matched via higher-order dispersion.

It also presents a localized shift in the longitudinal phase, which we will denote $\phi_{loc}(\xi, \tau)$ with respect to the background phase $\kappa_b \xi$.[36] This deviation, which can be seen as a phase anomaly arising from the nonlinear nature of the solution, is intrinsically associated to the localized pulse. Thus, the overall phase of the Peregrine soliton is the sum of the background phase and this local shift, which reads as

$$\begin{aligned} \phi_{PS}(\xi, \tau) &= \kappa_b \xi + \phi_{loc}(\xi, \tau) \\ &= \kappa_b \xi - \tan^{-1}\left(\frac{8\xi}{4\xi^2 + 4\tau^2 - 3}\right). \end{aligned} \tag{3}$$

Note that, even though the formula for the phase shift appears to present a jump whenever the denominator vanishes, it is just a consequence of absorbing a change of sign in the bracket in (2) which does not affect the conclusions, so we will ignore it for the sake of keeping the formulae simpler. The maximum anomaly is attained at the maximum amplitude of the peak ($\tau = 0$). The ξ-derivative at $\tau = 0$ provides the nonlinear wavenumber of the Peregrine soliton:

$$\begin{aligned} \kappa_{PS}(\xi) &= \kappa_b + \kappa_{loc}(\xi) \\ &= \kappa_b + \frac{4(8\xi^2 + 6)}{(4\xi^2 + 1)(4\xi^2 + 9)}, \end{aligned} \tag{4}$$

which similarly consists on the constant wavenumber of the background κ_b shifted by a local contribution $\kappa_{loc}(\xi)$. It tends asymptotically to κ_b as $\xi \to \pm\infty$, whereas the local contribution is stronger around $\xi = 0$.

A good estimation of the radiated frequencies can be provided by phase matching their wavenumber to that of the Peregrine soliton, $\kappa_{RR}(\omega) = \kappa_{PS}$, where κ_{RR} denotes the wavenumber of a linear component wave of the RR at a frequency detuning ω from the soliton. It is worth noting that for this estimation to be accurate, one must study κ_{RR} in a frame making the soliton stationary, hence we need to change to a moving frame with the velocity $v_p = d\tau/d\xi$ of the Peregrine soliton.

Now, to take into account the effects of the full equation (that is, $\sigma_1 \neq 0$, making the Peregrine solution an approximate one), we introduce linear waves of the form $\exp(i\kappa_{RR}\xi - i\omega\theta)$, where $\theta = \tau - v_p \xi$ denotes a retarded time in the moving frame, into Eq. (1), which, as one can easily check, obey the dispersion relation

$$\kappa_{RR}(\omega) = \frac{\sigma_1}{6}\omega^3 - \frac{1}{2}\omega^2 - v_p\omega, \tag{5}$$

This expression must however be completed by a nonlinear correction $\kappa_{RR}^{NL} = 2\kappa_b$ (which corresponds to $2\kappa_b z_{nl}^{-1} = 2\gamma P$ in real-world units) generated by the cross-phase modulation induced by the strong background, which serves as the medium in which the linear waves are generated and propagate. Equating the full form of κ_{RR} to the Peregrine wavenumber (4), we obtain the phase-matching condition

$$\frac{\sigma_1}{6}\omega^3 - \frac{1}{2}\omega^2 - v_p\omega = \Delta\kappa_{nl}, \tag{6}$$

where the term $\Delta\kappa_{nl} = \kappa_{PS} - 2\kappa_b = \kappa_{loc}(\xi) - \kappa_b$ sums up all the effective nonlinear contributions. The roots $\omega = \omega_{RR}$ of Eq. (6) provide the resonant frequencies, which correspond in real-world units to $\Omega_{RR} = \omega_{RR}/t_0 = \omega_{RR}(|\beta''|z_{nl})^{-1/2}$.
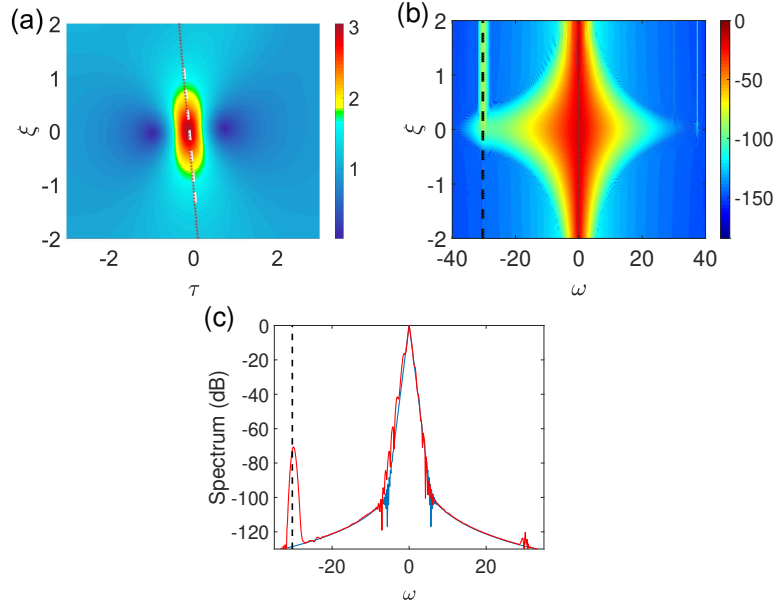
Figure 1: Propagation of a perturbed radiating Peregrine soliton in the cubic case with $\beta_1 = -1$ and $\sigma_1 = -0.1$: (a) pseudo-color plot of spatio-temporal evolution of the intensity $|\psi|^2$, the dashed white line and dotted red line mark the predicted and numerical Peregrine soliton velocity, respectively; (b) evolution of the Fourier spectrum (in log scale); (c) output spectrum (in log scale, solid red) at $\xi = 2$ superposed to the input spectrum (solid blue). In (b-c) the dashed black line shows the predicted RR frequency from Eq. (6).
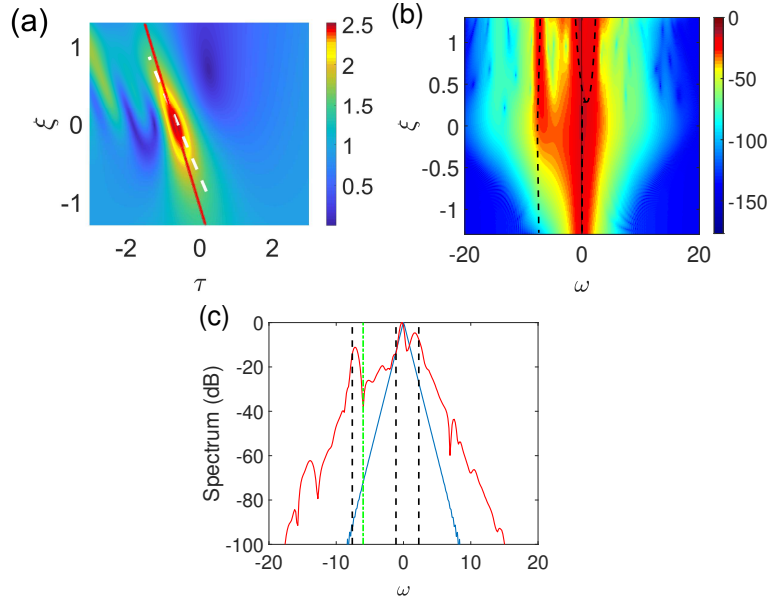
Figure 2: Same as Fig. 1 for stronger TOD $\sigma_1 = -0.5$. In (c) the three dashed black lines mark the three predicted RR frequencies, while the dashed green line marks the first-order approximation $\omega_{RR} \simeq 3/\sigma_1$.
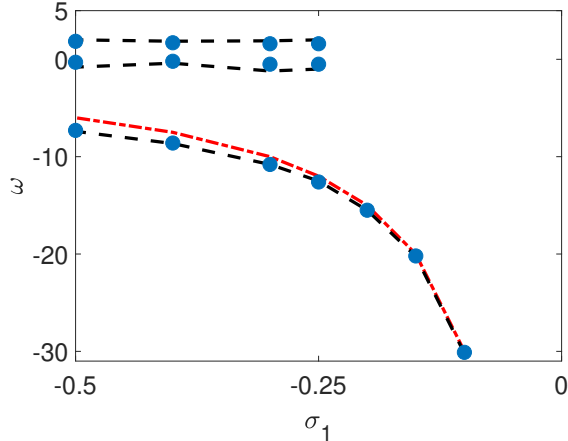
Figure 3: Impact of the third-order dispersion in the cubic case: frequencies ω_{RR1}, ω_{RR2} and ω_{RR3} against the normalized coefficient σ_1; blue dots: numerical data; black dashed lines: theoretical approximation from Eq. 6; red dashed line: first-order approximation $\tilde{\omega}_{RR} = 3/\sigma_1$.

Note that in order for the standard first-order approximation of the RR frequency, $\omega_{RR} \simeq 3/\sigma_1$, with corresponding physical frequency $\Omega_{RR} = 3|\beta''|/\beta'''$ (as also estimated from either solitons or wave-breaking [17, 27, 28]), we need both v_p and $\Delta\kappa_{nl}$ to be negligible. In any other case, the phase-matched RR involves the local wavenumber $\kappa_{loc}(\xi)$, unlike the case of both bright and dark solitons, while the sign of the nonlinear contribution κ_b changes as compared to the bright soliton case, [23], due to the strong background, similarly to the RR generated by shock waves.[26] It should also be noted that, in the anomalous dispersion regime the background plane waves are modulationally unstable and may eventually generate additional rogue wave-like peaks due to the introduced perturbations. However, the timespan of these ocurring is much longer than that of the emission of resonant radiation so for our purposes we will treat their effect as being negligible[63].

A typical scenario of RR is shown in Fig. 1, which depicts the Peregrine solution for $\sigma_1 = -0.1$, by launching the exact solution at $\xi = -2$ and integrating numerically Eq. (1) for its evolution. The RR is noticeable in Fig. 1(a), and even more so in the Fourier spectrum in Fig. 1(b). Note that the radiating Peregrine soliton drifts slightly with a constant velocity $v_p \neq 0$, which can be estimated by $v_p = \sigma_1 A^2/6$ (plotted in red), where A denotes the peak amplitude of the Peregrine soliton (in this case, $A \sim 3$ for a unit background). The numerical estimation for v_p is also shown in Fig. 1 by a dashed white line. Figure 1 shows that the RR is clearly in the normal dispersion regime and its emission starts when the spectrum of the Peregrine gets broadest, so that it can efficiently seed the frequency ω_{RR}. The latter can be estimated analytically as the only real root of Eq. (6). The merit of such estimation is demonstrated in Fig. 1(c), which superposes the analytical estimation (see dashed vertical line) to the spectrum of the solution at $\xi = 2$, which features a secondary peak corresponding to the resonant radiation. A similar analysis for stronger TOD $\sigma_1 = -0.5$ (see Fig. 2), shows that in this case three different frequencies appear (two of which being at much lower detunings), which correspond to the the real roots of Eq. (6). In this case the soliton exhibits a much stronger RR and a much faster drift.

The effect on the RR frequency of the variations of the TOD coefficient is summarized in Fig. 3, which report the outcome of different numerical simulations for multiple values of TOD. As shown, the main branch at large detuning ω_{RR1} exists for any value of TOD σ_1, whereas the low-frequency components only start to appear below a certain critical value $\sigma_1 \simeq -0.25$, beyond which their

frequency is almost invariant to the value of σ_1. Also note that we have taken the choice of negative σ_1 but positive values are completely equivalent provided the sign of the RR frequencies is reversed, thus yielding the same physics.

3 Quadratic media

A different situation occurs when dealing with quadratic media. Contrary to the cubic case, where higher-order dispersion is the driving mechanism that allows for RR to be phase-matched with the soliton, other mechanisms take place in quadratic media. Indeed, when one computes the equivalent of Eq. (6) for quadratic media in the cascading regime (where it is possible to reduce the equation to a cubic one) [55, 56], without higher-order dispersion, it turns out it has no real roots, thus predicting in principle no RR whatsoever. However, as we will see, a resonance driven by the optical second harmonic (SH) is able to initiate the radiative process which then involves also RR around the fundamental frequency (FF) through non-degenerate down-conversion processes [61]. Note that extensive numerical and physical experiments have explored the RR in quadratic media but always working under the interpretative hypothesis that the radiation is driven by higher-order dispersive terms [46, 47, 48, 49, 53, 54, 55, 56, 57, 58, 59, 60].

The dimensionless coupled equations for the pulse propagation in dispersive quadratic media are:[64, 46]

$$iu_{1\xi} - \frac{\beta_1}{2}u_{1\tau\tau} + u_2 u_1^* e^{-i\delta k\xi} = 0, \tag{7}$$

$$iu_{2\xi} + ivu_{2\tau} - \frac{\beta_2}{2}u_{2\tau\tau} + u_1^2 e^{i\delta k\xi} = 0, \tag{8}$$

where $u_{1,2}(\xi,\tau)$ are the normalized envelopes of the FF and generated SH in the FF group velocity frame, respectively. Here $\xi = z/z_d = z|\beta_1''|/t_0^2$ is the normalized propagation distance, where $z_d = t_0^2/|\beta_1''|$ is the dispersion length. $\tau = (t - z/v_1)/t_0$ is the time in the FF group velocity frame, $v = z_d/z_w$ is the ratio between the dispersion length and the temporal walk-off length $z_w = t_0/(v_2^{-1} - v_1^{-1})$, with $v_{1,2} = dk/d\omega|_{\omega_0,2\omega_0}^{-1}$. $\beta_{1,2}$ are the GVDs, with $\beta_1 = \text{sign}(\beta_1'')$, $\beta_2 = \beta_2''/|\beta_1''|$ where $\beta_{1,2}'' = d^2k/d\omega^2|_{\omega_0,2\omega_0}$. $\delta k = \Delta k z_d$ is the normalized wave number mismatch, where $\Delta k = 2k_1 - k_2$ with $k_{1,2} = k|_{\omega_0,2\omega_0}$. Furthermore, $u_{1,2} = \chi z_d A_{1,2}$, where $|A_{1,2}|^2$ measures the intensity, with $\chi = \omega_0[2/(c^3\epsilon_0 n_{\omega_0}^2 n_{2\omega_0})]^{1/2} d^{(2)}$ and $d^{(2)}$ is the nonlinear element.

3.1 Cascading regime

At large mismatches $|\delta k| \gg 1$ (the so-called cascading regime, where the quadratic nonlinearity mimics the cubic one [46]), by using the SH asymptotic expansion $u_2 = \sum_{n=0}^{\infty} u_2^{(n)}/\delta k^n$ and the method of repeated substitution [64], retaining leading-order terms, we arrive at a single FF evolution equation (obtained at $n = 2$ order):

$$i\rho_\xi - \frac{\beta_1}{2}\rho_{\tau\tau} + \kappa|\rho|^2\rho + i\gamma|\rho|^2\rho_\tau = 0, \tag{9}$$

where for simplicity we have defined $u_1 = \rho$, $u_2 \simeq \frac{1}{\delta k}\rho^2 e^{i\delta k\xi} + \frac{2iv}{\delta k^2}\rho\rho_\tau e^{i\delta k\xi}$, $\kappa = 1/\delta k$, and $\gamma = 2v/\delta k^2$. We emphasize that the mapping of the FF wave evolution of Eqs. (7) and (8) into Eq. (9) is only valid with large mismatch δk, and also with large walk-off v compared to dispersions $\beta_{1,2}$. Under such conditions, the role of the dispersion β_2 becomes negligible, and the SH wave evolution can be also dictated by Eq. (9) through the above mapping relation.

6

Eq. (9) is known as the integrable Chen-Lee-Liu (CLL) equation[65], which when $\gamma = 0$ reduces to the integrable NLS equation.

Therefore, we emphasize that approximate two-color quadratic solutions $[u_1(\tau, \xi), u_2(\tau, \xi)]$ (so called because of the FF and SH components) of CLL soliton type $\rho(\tau, \xi)$ can be written as:

$$
\begin{aligned}
u_1(\tau, \xi) &= \rho(\tau, \xi), \\
u_2(\tau, \xi) &= \frac{1}{\delta k}\rho(\tau, \xi)^2 e^{i\delta k\xi} + \frac{2iv}{\delta k^2}\rho(\tau, \xi)\rho(\tau, \xi)_\tau e^{i\delta k\xi}.
\end{aligned}
\tag{10}
$$

Using the CLL chirped Peregrine solution, obtained via a gauge transformation[66], one can write the quadratic Peregrine soliton as

$$
u_1(\tau, \xi) = \left[1 - \frac{2i\left(\frac{\gamma\theta}{\beta_1} + \kappa\xi\right) + 1}{\left(\kappa - \frac{\gamma^2}{\beta_1}\right)\left(\kappa\xi^2 - \frac{\theta^2}{\beta_1}\right) + \frac{1}{4} + i\frac{\gamma(\gamma\xi+\theta)}{\beta_1}}\right] e^{i\kappa\xi},
\tag{11}
$$

$$
u_2(\tau, \xi) = \kappa u_1^2(\tau, \xi) e^{i\delta k\xi} + 2iv\kappa^2 u_1(\tau, \xi)\, u_1(\tau, \xi)_\tau\, e^{i\delta k\xi},
\tag{12}
$$

where we have further defined $\theta = \gamma\xi - \tau$, subject to the constraint $\delta k\beta_1 < 0$, necessary for compensating GVD and nonlinearity. Note that the background of u_1 was set to have unit value without loss of generality. Different kinds of Peregrine solitons exist for various choices of the mismatch δk, the GVD β_1 and the walk-off v.[67, 68]

As expected, when reducing it to the focusing NLS equation via the choice of parameters $\gamma = 0$ and $\beta_1 = -1$, the Peregrine soliton component at the FF reads

$$
u_1(\tau, \xi) = \left[1 - \frac{4(1 + 2i\kappa\xi)}{1 + 4\kappa^2\xi^2 + 4\kappa\tau^2}\right] e^{i\kappa\xi},
\tag{13}
$$

which coincides with Eq. (2) except for the influence of the variable κ.

In general, one of the defining characteristics of solitons in integrable systems is that they do not couple energy into linear waves. However this fact usually does not hold when taking into consideration higher-order terms in the equation which breaks the integrability (and, in this case, soliton solutions may be only approximate solutions). Based on the fact that the existence of the Peregrine soliton is supported by the interplay between the Kerr-like nonlinearity and the GVD at the FF (where the integrable limit is represented by the NLS equation), we want to seek for RR generated by GVD of the same leading order at the SH in Eqs. (7-8).

RR generated by phase matching of this kind of solution was studied in Ref. [61]. For the FF component in Eq. (7), the condition for the presence of RR was found to be

$$
\frac{\beta_1}{2}\omega_1^2 - \omega_1 v_p = \kappa + \kappa_{loc},
\tag{14}
$$

where v_p is the velocity of the Peregrine soliton, $v_p = 2v/\delta k^2 (= \gamma)$, and

$$
\kappa_{loc} = \frac{8\kappa\beta_1 - 24\gamma^2}{3\beta_1},
\tag{15}
$$

while for the SH component in Eq. (8), the resonant condition was found to read as

$$
\frac{\beta_2}{2}\omega_2^2 - \omega_2(v_p - v) = \delta k + 2\kappa + 2\kappa_{loc}.
\tag{16}
$$
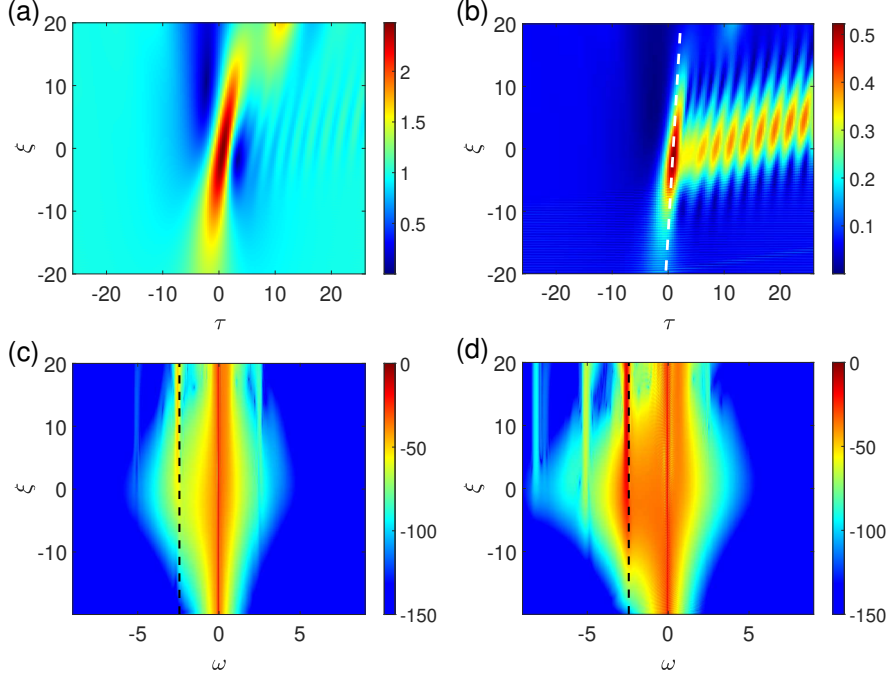
Figure 4: Pseudo-color plot of the spatio-temporal evolution of intensities (a) at FF $|u_1|^2$ and (b) at SH $|u_2|^2$ components of a typical walking Peregrine soliton in the (τ, ξ) plane. (c,d): corresponding evolution of the FF (c) and SH (d) Fourier spectra (in log scale); the dashed black line marks the predicted resonant frequencies $\omega^+_{1,FC}$ in (c) and $\omega^+_{2,RR}$ in (d). Here $\beta_1 = \beta_2 = 1$, $v = 7.5$, $\delta k = -15$.

In both cases the method employed to find such conditions was to look for matches between the wavenumber of potentially growing linear wave components of the form $\exp(i\kappa_{\mathrm{lin},\{1,2\}}\xi - i\omega_{1,2}\tau_p)$, where $\tau_p = \tau - v_p\xi$ corresponds to the Peregrine moving frame, with nonlinear wavenumbers κ_{nl} of the Peregrine soliton (i.e., similar to the cubic case [17, 18, 23], though taking into account linear waves around both the FF and the SH). This amounts to neglect nonlinear terms in the interaction between the linear waves and the soliton driving wavepackets. Note that, as compared with Ref. [61], we have added the local correction κ_{loc} due to nonlinearity for consistency with the derivation for the cubic case. However, as evidenced below by Eq. (17) and due to the fact that $|\delta k| \gg |\kappa_{loc}|$ in the cascading regime, its role in this analysis turns out to be negligible.

As expected, the condition on ω_1, Eq. (14), does not yield real solutions, consistently with the fact that, in the NLS equation, solitons are not in resonance with linear waves unless higher-order dispersion is present. Conversely, the condition on ω_2, Eq. (16), does yield real roots, which read

$$\omega^{\pm}_{2,RR} = \frac{(v_p - v) \pm \sqrt{(v_p - v)^2 + 2\beta_2(\delta k + 2\kappa + 2\kappa_{loc})}}{\beta_2}. \tag{17}$$

Similarly to the cubic case, such two resonant frequencies are not symmetric around the soliton frequency (they readily become symmetric for stationary solitons, $v_p = 0$, implying $v = 0$). Also note that, for small values of the group-velocity mismatch v, the constraint $\beta_1\beta_2 < 0$ holds, which requires GVDs of different signs. This constraint, however, is no longer required as the walk-off v increases. Indeed, for sufficiently large values of v, real solutions $\omega^{\pm}_{2,RR}$ do exist for GVDs of the same sign, as shown in the example of Fig. 4.

In Fig. 4(a) and (b) we display the evolution of a typical radiating Peregrine soliton in the

8
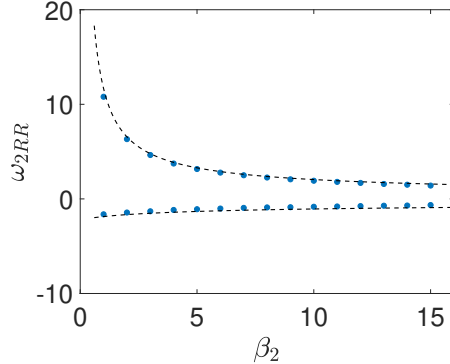
Figure 5: RR frequencies $\omega_{2,RR} = \omega_{2,RR}^{\pm}$ versus GVD at SH β_2 at $v = 5$, comparing theoretical predictions (dashed black curves) and numerical simulations (blue dots). Here $\beta_1 = -1$, $\delta k = 20$.

(τ, ξ) plane for both the FF and the SH, as obtained by integrating numerically Eqs. (7) - (8) with initial value given by the exact solution [Eqs. (11) - (12)] at $z = -30$. In Fig. 4(c) and (d) we show the corresponding Fourier spectral evolutions. In all this example we set $\beta_1 = \beta_2 = 1/2$, $v = 7.5$ and $\delta k = -15$ (and hence $\kappa = -1/15$ and $v_p = 1/15$). We see significant RR at the SH, emitted at the peak intensity of the Peregrine soliton at $z = 0$, preferentially towards positive times. The corresponding frequency detuning, highlighted in Fig. 4(d), is $\omega_{2,RR}^{+} = -2.4$. The other root, $\omega_{2,RR}^{-} = -12.4$ is too far detuned to have a noticeable effect on the spectrum.

Once the RR is emitted around the SH, a corresponding radiation arounds the FF can be generated via frequency conversion processes of non-degenerate downconversion type, which can be described as follows. By conveniently introducing the real-world detunings $\Omega_{1,2} = t_0^{-1}\omega_{1,2}$, the RR detuned from the SH by $\Omega_{2,RR}^{\pm}$ corresponds to photons at physical pulsations $2\omega_0 + \Omega_{2,RR}^{\pm}$. Such photons can mix through three-photon difference frequency conversion processes $(2\omega_0 + \Omega_{2,RR}^{\pm}) - \omega_0 = \omega_0 + \Omega_{1,FC}^{\pm}$. The conservation of energy, implies equal detunings from the FF and the SH, that is, $\Omega_{1,FC}^{\pm} = \Omega_{2,RR}^{\pm}$. The RR around the FF, having secondary origin through down-conversion, turns out to be weaker than that around the SH, but is nevertheless quite prominent as shown in Fig. 4(c). In this case, in terms of the normalized frequencies, we find $\omega_{1,FC}^{+} = \omega_{2,RR}^{+} = -2.4$, which agrees quite well with the RR observed numerically in Fig. 4(c,d). We emphasize that the radiative mechanism turns out to be quite efficient, as the spectrum peaks at the resonant frequency reach values comparable to those of the Peregrine peak, especially in the SH case.

Additionally, we can study the effect on the resonant frequencies of varying the parameters of the model. Looking at Eq. (17), it only presents real roots if

$$\beta_2 \geq -\frac{(v_p - v)^2}{2(\delta k + 2\kappa + 2\kappa_{loc})} \approx -\frac{v^2}{2\delta k} \ . \tag{18}$$

In Fig. 5 we summarize the outcome of numerical simulations in the range of $\beta_2 > 0$ at $v = 5$ (other parameters in the caption). In this case, the dominant (negative) frequency stays nearly constant with β_2, while the other frequency, turns out to be much more sensitive to β_2. As the value of β_2 is reduced below a certain threshold, the RR frequency becomes too large to be noticeably excited since the RR is no longer efficiently seeded by the spectral broadening of the soliton.

Finally, we can study how the walk-off affects the RR by varying v under a set of fixed parameters. As shown by Eq. (18), for $\beta_2 > 0$ (normal GVD) there always exist real roots irrespective of the

9
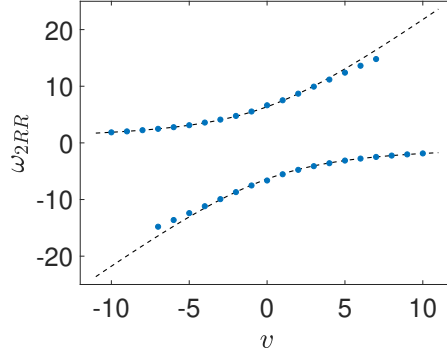
Figure 6: RR frequencies versus normalized walk-off v, for $\beta_2 = 1$, comparing theoretical prediction (dashed black curves) with numerical simulations (blue dots). Here $\beta_1 = -1$, $\delta k = 20$.
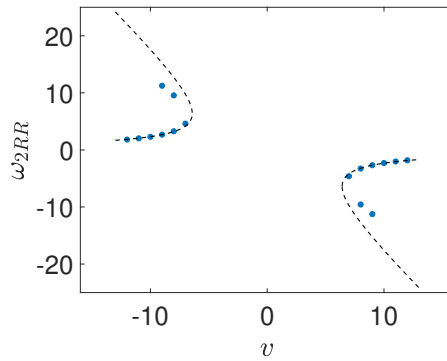
Figure 7: As in Fig. 6 for $\beta_2 = -1$. Here $\beta_1 = -1$, $\delta k = 20$.

value of v. However, when $\beta_2 < 0$ (anomalous GVD) real roots exist only under the (approximate) condition

$$|v| > v_{min} \approx \sqrt{2\delta k |\beta_2|}.$$

(19)

Figure 6 shows the variation of the radiated frequency with v for normal GVD at SH ($\beta_2 = 1$). The frequency pair is situated centrosymmetrically with respect to $v = 0$. Numerically, the frequency pair is excited in the range $|v| < 7$, beyond which one of the frequencies is too far from the Peregrine soliton to be excited.

Figure 7 shows the variation for the same parameters except for an anomalous GVD at SH ($\beta_2 = -1$). As shown a gap in walk-off exists, i.e. $|v| < \sqrt{40}$, where the quadratic Peregrine soliton is not resonant with dispersive waves. Interestingly, in this case both resonant frequencies for the same choice of parameters stand on one side of the pump frequency, both positive when $v < 0$ and both negative when $v > 0$.

3.2 Non-cascading regime

We will now move on to study Peregrine solitons without resorting to the cascading regime. For that, we will consider an anomalous GVD $\beta_1 = -1$ for the FF and a normal GVD $\beta_2 > 0$ for the SH. In this framework, the resulting Peregrine solitons will be still localized on both time and space, and

they will present a peak position with more than twice the amplitude of the background.[34, 40, 41] This Peregrine solution of Eqs. (7) and (8) can be approximated as[34, 40, 45]

$$u_1(\xi, \tau) = A \left[1 - \frac{2i\gamma\xi + 1/A^2}{\gamma\theta^2 + \gamma^2 A^2 \xi^2 + 1/(4A^2)} \right] \exp\left[i(\kappa\xi - \Omega\theta)\right], \tag{20}$$

$$u_2(\xi, \tau) = \gamma u_1^2 e^{i\delta k \xi}, \tag{21}$$

where A is the amplitude of the background, $\theta = \tau - v_p \xi$,

$$v_p = \frac{v\beta_1}{\beta_1 - 2\beta_2}, \quad \kappa = \gamma A^2 - \frac{v_p^2}{2\beta_1}, \quad \Omega = \frac{v_p}{\beta_1}, \tag{22}$$

and

$$\gamma = \frac{vv_p - \beta_1 \delta k - \sqrt{8A^2\beta_1^2 + (vv_p - \beta_1 \delta k)^2}}{4A^2 \beta_1}. \tag{23}$$

Proceeding as in the cascading limit, we introduce plane waves of the form $\exp(i\kappa_{\text{lin},\{1,2\}}\xi - i\omega_{1,2}\tau_p)$ and equate their wavenumber to that of the nonlinear waves, $\kappa_{\text{lin},1} = \kappa + \kappa_{loc}$, $\kappa_{\text{lin},2} = \delta k + 2\kappa + 2\kappa_{loc}$ (also known as the phase-matching condition for the RR),[23] where the local correction κ_{loc} reads

$$\kappa_{loc} = \frac{8A^2\gamma}{3}. \tag{24}$$

The resulting conditions read

$$\gamma A^2 - \frac{v_p^2}{2\beta_1} = \frac{\beta_1 \omega_1^2}{2} - \omega_1 v_p, \tag{25}$$

$$\delta k + 2\gamma A^2 - \frac{v_p^2}{\beta_1} = \frac{\beta_2 \omega_2^2}{2} + \omega_2(v - v_p). \tag{26}$$

Also similarly to the previous case, the condition for the FF component does not yield real roots whereas frequencies must be real quantities. Therefore the RR will be generated via frequency down-conversion from the RR driven by the SH, which admits the real roots

$$\omega_2^\pm = \frac{2v_p}{\beta_1} \pm \sqrt{\frac{2(2A^2\beta_1\gamma - vv_p + \beta_1\delta k)}{\beta_1\beta_2}}. \tag{27}$$

Applying a process analogous to the one employed in the cascading limit, the down-converted RR around the FF is found to occur at frequencies

$$\omega_1^+ = \frac{3\omega_2^+ - \omega_2^-}{4}, \quad \omega_1^- = \frac{3\omega_2^- - \omega_2^+}{4}. \tag{28}$$

Note that both for the FF and the SH the resonant frequencies are located symetrically with respect to the central frequencies $\Omega = v_p/\beta_1$ and $2\Omega = 2v_p/\beta_1$, respectively.

In Fig. 8 we show the RR of a Peregrine soliton under the phase-matched condition $\delta k = 0$, with a large temporal walk-off $v = 3$. The analytic solutions presented above are consistent with the numerical results, even in the central peak, which exhibits the higher compression. Strong RR appear after the central peak $\xi = 0$, both in the SH component and later on in the FF component via downconversion. Its frequency is consistent with our predictions, which for these values of the

11
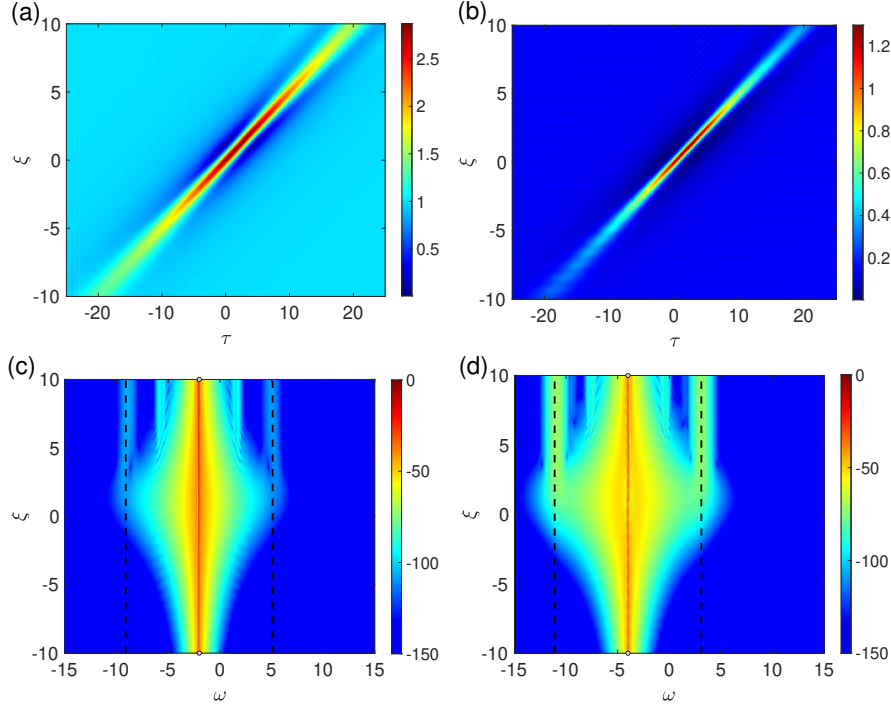
Figure 8: Optical RR emitted by the PS under phase-matching $\delta k = 0$, with a large temporal walk-off $v = 3$, $\beta_1 = -1$, $\beta_2 = 1/4$ and $A = 1$. (a,b): Temporal evolutions of intensities at FF, SH, respectively; (c,d): spectral (log scale) evolutions at FF, SH, respectively, compared with predictions (dashed black vertical lines) from Eqs. (24-25).

parameters translate into $\omega_2^+ = 3.11$ and $\omega_2^- = -11.11$ for the SH, and $\omega_1^+ = 5.11$ and $\omega_1^- = -9.11$ for the FF, which are highlighted by the dashed vertical black lines in Fig. 8(c) and (d).

This strong RR may be related to the transient property of the Peregrine solitons, which undergoes and intense compression at the peak to then radiate as it recovers from it. It is worth noting that more resonant frequencies that are not predicted by our computations appear in Fig. 8(c) and (d), which require further research.

4 Conclusions

To summarize, we have provided our recent advances in understanding the RR emitted by Peregrine solitons in either cubic or quadratic media, with extra new numerical simulations.

In the case of cubic media, we have shown that Peregrine solitons can emit linear dispersive waves at certain resonant frequencies in presence of higher-order dispersion, similarly to the case with classical bright and dark solitons. However, unlike the latter soliton case, the radiated frequency can be effectively affected by the local contribution to the intrinsic wavenumber of the Peregrine soliton. This contribution is not unique to the Peregrine soliton, instead it is shared by other kinds of rogue-type solutions, in particular, Akhmediev breathers and Kuznetsov-Ma solitons, possibly describing other rogue wave dynamics.

In the case of quadratic media, our results offer a wider perspective of the phenomenon of soliton RR, showing that it can be driven by the GVD of the SH component and then occurs simultaneously on the FF component as well via concomitant difference-frequency generation processes. Our

analytical criterion obtained from the phase-matching condition can accurately predict the resonant frequencies at which the linear dispersive waves are emitted. Different from other RR mechanisms, typically driven by higher-order dispersions, the present mechanism can also be employed for the case of spatial solitary waves, which are described by coupled second-harmonic generation equations but with anomalous GVD replaced by the spatial diffraction. Thus, the introduced mechanism can lead to a rare case of radiating spatial solitons, as well as induce reshaping of the spectrum of spatio-temporal bullets in bulk media.

Acknowledgments

References

[1] M. A. Eftekhar, H. Lopez-Aviles, F. W. Wise, R. Amezcua-Correa, and D. N. Christodoulides, "General theory and observation of Cherenkov radiation induced by multimode solitons," *Commun. Phys.*, vol. 4, p. 137, 2021.

[2] M. Zhang, W. Wang, T. Xian, and L. Zhan, "Real-time revealing of Cherenkov radiation evolution in optical fibers," *Opt. Lett.*, vol. 48, pp. 3343–3346, 2023.

[3] E. Rubino, J. McLenaghan, S. C. Kehr, F. Belgiorno, D. Townsend, S. Rohr, C. E. Kuklewicz, U. Leonhardt, F. König, and D. Faccio, "Negative-frequency resonant radiation," *Phys. Rev. Lett.*, vol. 108, p. 253901, 2012.

[4] M. Chemnitz, R. Scheibinger, C. Gaida, M. Gebhardt, F. Stutzki, S. Pumpe, J. Kobelke, A. Tünnermann, J. Limpert, and M. A. Schmidt, "Thermodynamic control of soliton dynamics in liquid-core fibers," *Optica*, vol. 5, no. 6, pp. 695–703, 2018.

[5] D. V. Skryabin, Y. V. Kartashov, O. A. Egorov, M. Sich, J. K. Chana, L. E. Tapia Rodriguez, P. M. Walker, E. Clarke, B. Royall, M. S. Skolnick, and D. N. Krizhanovskii, "Backward Cherenkov radiation emitted by polariton solitons in a microcavity wire," *Nat. Commun.*, vol. 8, p. 1554, 2017.

[6] W. R. Rowe, D. V. Skryabin, and A. V. Gorbach, "Temporal quadratic solitons and their interaction with dispersive waves in lithium niobate nanowaveguides," *Phys. Rev. Res.*, vol. 1, p. 033146, 2019.

[7] A. V. Gorbach, W. Ding, O. K. Staines, C. E. de Nobriga, G. D. Hobbs, W. J. Wadsworth, J. C. Knight, D. V. Skryabin, A. Samarelli, M. Sorel, and R. M. de la Rue, "Spatiotemporal nonlinear optics in arrays of subwavelength waveguides," *Phys. Rev. A*, vol. 82, p. 041802(R), 2010.

[8] J. K. Jang, M. Erkintalo, S. G. Murdoch, and S. Coen, "Observation of dispersive wave emission by temporal cavity solitons," *Opt. Lett.*, vol. 39, no. 19, pp. 5503–5506, 2014.

[9] S. Malaguti, M. Conforti, and S. Trillo, "Dispersive radiation induced by shock waves in passive resonators," *Opt. Lett.*, vol. 39, no. 19, pp. 5626–5629, 2014.

[10] B. Yao, S.-W. Huang, Y. Liu, A. K. Vinod, C. Coi, M. Hoff, Y. Li, M. Yu, Z. Feng, D.-L. Kwong, Y. Huang, Y. Rao, and X. Duan, "Gate-tunable frequency combs in graphene-nitride microresonators," *Nature*, vol. 558, pp. 410–414, 2018.

[11] Q.-F. Yang, X. Yi, K. Y. Yang, and K. Vahala, "Spatial-mode-interaction-induced dispersive waves and their active tuning in microresonators," *Optica*, vol. 3, no. 10, pp. 1132–1135, 2016.

[12] J. M. Dudley, G. Genty, and S. Coen, "Supercontinuum generation in photonic crystal fiber," *Rev. Mod. Phys.*, vol. 78, pp. 1135–1184, 2006.

[13] D. V. Skryabin and A. V. Gorbach, "Colloquium: Looking at a soliton through the prism of optical supercontinuum," *Rev. Mod. Phys.*, vol. 82, no. 2, pp. 1287–1299, 2010.

[14] V. Brasch, M. Geiselmann, T. Herr, G. Lihachev, M. H. P. Pfeiffer, M. L. Gorodetsky, and T. J. Kippenberg, "Photonic chip-based optical frequency comb using soliton Cherenkov radiation," *Science*, vol. 351, p. 6271, 2016.

[15] Y. Okawachi, K. Saha, J. S. Levy, Y. H. Wen, M. Lipson, and A. L. Gaeta, "Octave-spanning frequency comb generation in a silicon nitride chip," *Opt. Lett.*, vol. 36, no. 17, pp. 3398–3400, 2011.

[16] X. Guo, C.-L. Zou, H. Jung, Z. Gong, A. Bruch, L. Jiang, and H. X. Tang, "Efficient generation of a near-visible frequency comb via Cherenkov-like radiation from a Kerr microcomb," *Phys. Rev. Appl.*, vol. 10, p. 014012, 2018.

[17] P. K. Wai, C. R. Menyuk, Y. C. Lee, and H. H. Chen, "Nonlinear pulse propagation in the neighborhood of the zero-dispersion wavelength of monomode optical fibers," *Opt. Lett.*, vol. 11, no. 7, pp. 464–466, 1986.

[18] V. I. Karpman, "Radiation by solitons due to higher-order dispersion," *Phys. Rev. E*, vol. 47, no. 3, pp. 2073–2082, 1993.

[19] V. V. Afanasjev, Y. S. Kivshar, and C. R. Menyuk, "Effect of third-order dispersion on dark solitons," *Opt. Lett.*, vol. 21, pp. 1975–1977, Dec 1996.

[20] S. Roy, S. K. Bhadra, and G. P. Agrawal, "Effects of higher-order dispersion on resonant dispersive waves emitted by solitons," *Opt. Lett.*, vol. 34, no. 13, pp. 2072–2074, 2009.

[21] C. Milián and D. V. Skryabin, "Soliton families and resonant radiation in a micro-ring resonator near zero group-velocity dispersion," *Opt. Express*, vol. 22, no. 3, pp. 3732–3739, 2014.

[22] F. Baronio, S. Chen, and S. Trillo, "Resonant radiation from Peregrine solitons," *Opt. Lett.*, vol. 45, no. 2, pp. 427–430, 2020.

[23] N. Akhmediev and M. Karlsson, "Cherenkov radiation emitted by solitons in optical fibers," *Phys. Rev. A*, vol. 51, no. 3, pp. 2602–2607, 1995.

[24] M. Erkintalo, Y. Q. Xu, S. G. Murdoch, J. M. Dudley, and G. Genty, "Cascaded phase matching and nonlinear symmetry breaking in fiber frequency combs," *Phys. Rev. Lett.*, vol. 109, p. 223904, 2012.

14

[25] J. M. Soto-Crespo, A. Ankiewicz, N. Devine, and N. Akhmediev, "Modulation instability, Cherenkov radiation, and Fermi-Pasta-Ulam recurrence," *J. Opt. Soc. Am. B*, vol. 29, no. 8, pp. 1930–1936, 2012.

[26] M. Conforti and S. Trillo, "Radiative effects driven by shock waves in cavity-less four-wave mixing combs," *Opt. Lett.*, vol. 39, no. 19, pp. 5760–5763, 2014.

[27] K. E. Webb, Y. Q. Xu, M. Erkintalo, and S. G. Murdoch, "Generalized dispersive wave emission in nonlinear fiber optics," *Opt. Lett.*, vol. 38, no. 2, pp. 151–153, 2013.

[28] M. Conforti and S. Trillo, "Dispersive wave emission from wave breaking," *Opt. Lett.*, vol. 38, no. 19, pp. 3815–3818, 2013.

[29] M. Conforti, F. Baronio, and S. Trillo, "Resonant radiation shed by dispersive shock waves," *Phys. Rev. A*, vol. 89, p. 013807, 2014.

[30] M. Conforti, S. Trillo, A. Mussot, and A. Kudlinski, "Parametric excitation of multiple resonant radiations from localized wavepackets," *Sci. Rep.*, vol. 5, p. 9433, 2015.

[31] K. Krupa, A. Tonello, A. Berthélémy, V. Couderc, B. M. Shalaby, A. Bendahmane, G. Millot, and S. Wabnitz, "Observation of geometric parametric instability induced by the periodic spatial self-imaging of multimode waves," *Phys. Rev. Lett.*, vol. 116, p. 183901, 2016.

[32] A. U. Nielsen, B. Garbin, S. Coen, S. G. Murdoch, and M. Erkintalo, "Emission of intense resonant radiation by dispersion-managed Kerr cavity solitons," *APL Photonics*, vol. 3, p. 120804, 2018.

[33] D. H. Peregrine, "Water waves, nonlinear Schrödinger equations and their solutions," *J. Aust. Math. Soc. Series B Appl. Math.*, vol. 25, no. 1, pp. 16–43, 1983.

[34] B. Kibler, J. Fatome, C. Finot, G. Millot, F. Dias, G. Genty, N. Akhmediev, and J. M. Dudley, "The Peregrine soliton in nonlinear fibre optics," *Nat. Phys.*, vol. 6, pp. 790–795, 2010.

[35] H. Bailung, S. K. Sharma, and Y. Nakamura, "Observation of peregrine solitons in a multi-component plasma with negative ions," *Phys. Rev. Lett.*, vol. 107, p. 255005, 2011.

[36] G. Xu, K. Hammani, A. Chabchoub, J. M. Dudley, B. Kibler, and C. Finot, "Phase evolution of Peregrine-like breathers in optics and hydrodynamics," *Phys. Rev. E*, vol. 99, p. 012207, 2019.

[37] D. R. Solli, C. Ropers, P. Koonath, and B. Jalali, "Optical rogue waves," *Nature*, vol. 450, pp. 1054–1057, 2007.

[38] J. M. Dudley, F. Dias, M. Erkintalo, and G. Genty, "Instabilities, breathers and rogue waves in optics," *Nat. Photonics*, vol. 8, pp. 755–764, 2014.

[39] M. Onorato, S. Residori, U. Bortolozzo, A. Montina, and F. T. Arecchi, "Rogue waves and their generating mechanisms in different physical contexts," *Phys. Rep.*, vol. 528, no. 2, pp. 47–89, 2013.

[40] S. Chen, F. Baronio, J. M. Soto-Crespo, P. Grelu, and D. Mihalache, "Versatile rogue waves in scalar, vector, and multidimensional nonlinear systems," *J. Phys. A: Math. Theor.*, vol. 50, p. 463001, 2017.

[41] S. Chen, Y. Ye, J. M. Soto-Crespo, P. Grelu, and F. Baronio, "Peregrine solitons beyond the threefold limit and their two-soliton interactions," *Phys. Rev. Lett.*, vol. 121, p. 104101, 2018.

[42] S. Chen, L. Bu, C. Pan, C. Hou, F. Baronio, P. Grelu, and N. Akhmediev, "Modulation instability–rogue wave correspondence hidden in integrable systems," *Commun. Phys.*, vol. 5, no. 297, 2022.

[43] A. Tikan, C. Billet, G. El, A. Tovbis, M. Bertola, T. Sylvestre, F. Gustave, S. Randoux, C. Szwaj, and S. Bielawski, "Universality of the Peregrine soliton in the focussing dynamics of the cubic nonlinear Schrödinger equation," *Phys. Rev. Lett.*, vol. 119, p. 033901, 2017.

[44] R. Driben, A. V. Yulin, and A. Efimov, "Resonant radiation from oscillating higher-order solitons," *Opt. Express*, vol. 23, no. 15, pp. 19112–19117, 2015.

[45] L. Bu, G. Wu, C. Hou, S. Chen, P. Grelu, and F. Baronio, "Soliton resonant radiation in phase-matched second harmonic generation," *Phys. Rev. A*, vol. 109, p. 013510, 2024.

[46] A. V. Buryak, P. Di Trapani, D. V. Skryabin, and S. Trillo, "Optical solitons due to quadratic nonlinearities: from basic physics to futuristic applications," *Phys. Rep.*, vol. 370, no. 2, pp. 63–235, 2002.

[47] P. Di Trapani, D. Caironi, G. Valiulis, A. Dubietis, R. Danielius, and A. Piskarskas, "Observation of temporal solitons in second-harmonic generation with tilted pulses," *Phys. Rev. Lett.*, vol. 81, no. 3, pp. 570–573, 1998.

[48] X. Liu, L.-J. Qian, and F. W. Wise, "High-energy pulse compression by use of negative phase shifts produced by the cascade $\chi^{(2)} : \chi^{(2)}$ nonlinearity," *Opt. Lett.*, vol. 24, no. 23, pp. 1777–1779, 1999.

[49] S. Ashihara, J. Nishina, T. Shimura, and K. Kuroda, "Soliton compression of femtosecond pulses in quadratic media," *J. Opt. Soc. Am. B*, vol. 19, no. 10, pp. 2505–2510, 2002.

[50] J. Moses and F. W. Wise, "Soliton compression in quadratic media: high-energy few-cycle pulses with a frequency-doubling crystal," *Opt. Lett.*, vol. 31, no. 12, pp. 1881–1883, 2006.

[51] M. Marangoni, C. Manzoni, R. Ramponi, G. Cerullo, F. Baronio, C. De Angelis, and K. Kitamura, "Group-velocity control by quadratic nonlinear interactions," *Opt. Lett.*, vol. 31, no. 4, pp. 534–536, 2006.

[52] F. Bache, O. Bang, J. Moses, and F. W. Wise, "Nonlocal explanation of stationary and nonstationary regimes in cascaded soliton pulse compression," *Opt. Lett.*, vol. 32, no. 17, pp. 2490–4292, 2007.

[53] F. Bache, O. Bang, B. B. Zhou, and F. W. Wise, "Optical Cherenkov radiation in ultrafast cascaded second-harmonic generation," *Phys. Rev. A*, vol. 82, p. 063806, 2010.

[54] B. Zhou, A. Chong, F. W. Wise, and M. Bache, "Ultrafast and octave-spanning optical nonlinearities from strongly phase-mismatched quadratic interactions," *Phys. Rev. Lett.*, vol. 118, p. 043902, 2012.

[55] M. Conforti, N. Westerberg, F. Baronio, S. Trillo, and D. Faccio, "Negative-frequency dispersive wave generation in quadratic media," *Phys. Rev. A*, vol. 88, p. 013829, 2013.

[56] B. Zhou, H. Guo, and M. Bache, "Soliton-induced nonlocal resonances observed through high-intensity tunable spectrally compressed second-harmonic peaks," *Phys. Rev. A*, vol. 90, p. 013823, 2014.

[57] B. Zhou, H. Guo, and M. Bache, "Energetic mid-IR femtosecond pulse generation by self-defocusing soliton-induced dispersive waves in a bulk quadratic nonlinear crystal," *Opt. Express*, vol. 23, no. 5, pp. 6924–6936, 2015.

[58] B. Zhou and M. Bache, "Dispersive waves induced by self-defocusing temporal solitons in a beta-barium-borate crystal," *Opt. Lett.*, vol. 40, no. 18, pp. 4257–4260, 2015.

[59] B. Zhou and M. Bache, "Multiple-octave spanning high-energy mid-IR supercontinuum generation in bulk quadratic nonlinear crystals," *APL Photonics*, vol. 1, p. 050802, 2016.

[60] B. Zhou, X. Liu, H. Guo, X. Zeng, X. F. Chen, H. P. Chung, Y. H. Chen, and M. Bache, "Parametrically tunable soliton-induced resonant radiation by three-wave mixing," *Phys. Rev. Lett.*, vol. 118, p. 143901, 2017.

[61] L. Bu, F. Baronio, S. Chen, and S. Trillo, "Quadratic Peregrine solitons resonantly radiating without higher-order dispersion," *Opt. Lett.*, vol. 47, no. 10, pp. 2370–2373, 2022.

[62] L. Bu, S. Chen, F. Baronio, and S. Trillo, "Resonant radiation emitted by solitary waves via cascading in quadratic media," *Opt. Express*, vol. 31, no. 5, pp. 8307–8324, 2023.

[63] P. K. Newton and J. B. Keller, "Stability of periodic plane waves," *SIAM J. Appl. Math.*, vol. 47, no. 5, pp. 959–964, 1987.

[64] R. Menyuk, R. Schiek, and L. Torner, "Solitary waves due to $\chi^{(2)} : \chi^{(2)}$ cascading," *J. Opt. Soc. Am. B*, vol. 11, no. 12, pp. 2434–2443, 1994.

[65] H. H. Chen, Y. C. Lee, and C. S. Liu, "Integrability of nonlinear Hamiltonian systems by inverse scattering method," *Phys. Scr.*, vol. 20, no. 3–4, pp. 490–492, 1979.

[66] S. Chen, F. Baronio, J. M. Soto-Crespo, Y. Liu, and P. Grelu, "Chirped Peregrine solitons in a class of cubic-quintic nonlinear Schrödinger equations," *Phys. Rev. E*, vol. 93, p. 062202, 2016.

[67] F. Baronio, "Akhmediev breathers and Peregrine solitary waves in quadratic medium," *Opt. Lett.*, vol. 42, no. 9, pp. 1756–1759, 2017.

[68] F. Baronio, S. Chen, and D. Mihalache, "Two-color walking Peregrine solitary waves," *Opt. Lett.*, vol. 42, no. 18, pp. 3514–3517, 2017.

17